Atomic properties calculated by relativistic coupled-cluster theory without truncation: Hyperfine constants of Mg$^+$, Ca$^+$, Sr$^+$, and Ba$^+$

B. K. Mani and D. Angom

Physical Research Laboratory, Navarangpura 380009, Gujarat, India

We demonstrate an iterative scheme for coupled-cluster property calculations without truncating the dressed properties operator. For validation, magnetic dipole hyperfine constants of alkaline-earth-metal ions are calculated using relativistic coupled-cluster theory and the role of electron correlation is examined. Then a detailed analysis of the higher-order terms is carried out. Based on the results, we arrive at an optimal form of the dressed operator, which we recommend for properties calculations with relativistic coupled-cluster theory.

I. INTRODUCTION

Coupled-cluster theory, first developed in nuclear many-body physics [1,2], is considered one of the best many-body theories. In recent times, it has been used with great success in nuclear [3], atomic [4,5], molecular [6], and condensed-matter [7] calculations. In atoms it is equivalent to incorporating electron correlation effects to all orders. It has been used extensively in precision atomic properties and structure calculations. These include atomic electric dipole moments [4,8], parity nonconservation [9], hyperfine structure constants [5,10], and electromagnetic transition properties [11,12].

Despite the remarkable developments and numerous calculations based on relativistic coupled-cluster theory, hitherto, a systematic analysis of the properties calculations with coupled-cluster wave functions has been lacking. This issue arises from the fact that the expression for properties with coupled-cluster wave functions is a nonterminating series. In this article we demonstrate an iterative scheme for calculating properties without truncation. Such a study is essential and timely as precision atomic calculations, in several instances, complement precision atomic experiments. These have direct bearing on, among other things, fundamental physics and new technology.

To test and validate the scheme, we employ open-shell coupled-cluster theory [13–15] and calculate the magnetic dipole hyperfine constants of alkaline-earth-metal ions ^{25}Mg$^+$, ^{43}Ca$^+$, ^{87}Sr$^+$, and ^{137}Ba$^+$. We have selected these ions as these are potential candidates for ongoing or proposed experiments. In addition, there is a large variation in the role of electron correlation among the ions and states. The ground-state hyperfine constant of Mg$^+$ is well studied with ion-trapping techniques [16]. The clock states of the next ion in the group, ^{43}Ca$^+$, were recently employed for high-fidelity entanglement [17], a crucial step in quantum information processing. Then, single trapped ^{87}Sr$^+$ is a suitable frequency standard [18]. These are application-oriented precision experiments. The other fascinating prospect is the observation of parity nonconservation in a single ^{137}Ba$^+$ [19]. In all of these endeavors, hyperfine interaction is involved. For this reason, several theoretical calculations have examined the role of electron correlations to the hyperfine constants of these ions. These provide a wealth of data for comparative study. In addition to the magnetic hyperfine constant, we also compute the excitation energies of the low-lying states. This is to verify the quality of the single-particle wave function we use.

The article is divided into seven sections. In Sec. II, we give a brief description of single-valence coupled-cluster theory. Section III is a short writeup on hyperfine interaction and how it is calculated with relativistic coupled-cluster theory. Section IV forms the core of the article, where we explain our iterative scheme to calculate properties with relativistic coupled-cluster theory to all orders. The details of the numerical methods and schemes used in the present work are provided in Sec. V. We present our results in Sec. VI. Finally, in Sec. VII we make concluding remarks, which may serve as guideline for any properties calculations with relativistic coupled-cluster theory. In the article, all the calculations and mathematical expressions are in atomic units ($e = \hbar = m_e = 1$).

II. SINGLE-VALENCE COUPLED-CLUSTER THEORY

For completeness and easy reference of the working equations, we provide a condensed overview of the single-valence coupled-cluster theory. Readers are referred to Ref. [15] for a detailed exposition of the theory. In the Fock space coupled-cluster theory of single-valence systems, the correlated wave function is calculated in two steps. First, the cluster operators of the core electrons, or the closed-shell part T, are evaluated from the reference state $|\Phi_0\rangle$. Second, the cluster operators of the valence shells S are evaluated and the reference state is

$$|\Phi_v\rangle = a_v^\dagger|\Phi_0\rangle. \qquad (1)$$

The coupled-cluster wave function of the open shell system is

$$|\Psi_v\rangle = e^{T+S}|\Phi_v\rangle. \qquad (2)$$

For single-valence system $e^S = 1 + S$, the higher-order terms in the exponential do not contribute. Then

$$|\Psi_v\rangle = e^T(1 + S)|\Phi_v\rangle. \qquad (3)$$

For an N electron atom, the cluster operators are

$$T = \sum_{i=1}^{N-1} T_i \quad \text{and} \quad S = \sum_{i=1}^{N} S_i. \qquad (4)$$

Here the summation index of the T is up to the $N-1$ core electrons, whereas S is up to N to include the valence electron. However, single and double are the most dominant, in coupled-cluster single and double (CCSD) approximations
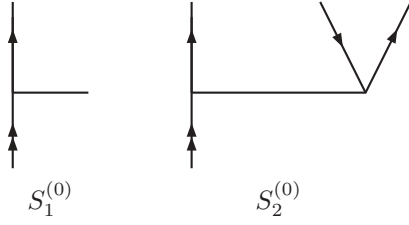
FIG. 1. Diagrammatic representation of open-shell cluster operators. The orbital lines with double arrows indicate valence and single up (down) arrow indicate particle (hole) states.

$T = T_1 + T_2$ and $S = S_1 + S_2$. In the second quantized representation, for the closed-shell part,

$$T_1 = \sum_{a,p} t_a^p a_p^\dagger a_a \quad \text{and} \quad T_2 = \frac{1}{2!} \sum_{a,b,p,q} t_{ab}^{pq} a_p^\dagger a_q^\dagger a_b a_a. \quad (5)$$

Similarly, for the valence shell,

$$S_1 = \sum_p s_v^p a_p^\dagger a_v \quad \text{and} \quad S_2 = \sum_{a,p,q} s_{va}^{pq} a_p^\dagger a_q^\dagger a_a a_v. \quad (6)$$

Here, $t^{\cdots}_{\cdots}$ and $s^{\cdots}_{\cdots}$ are the cluster amplitudes. The indexes $abc\ldots$ ($pqr\ldots$) represent core (virtual) states and $vwx\ldots$ represent valence states. The operators T_1 (S_1) and T_2 (S_2) give single and double replacements after operating on the closed-(open-)shell reference states. Diagrammatic representations of S are shown in Fig. 1.

The atomic state $|\Psi_v\rangle$ satisfies the eigenvalue equation

$$H|\Psi_v\rangle = E_v|\Psi_v\rangle, \quad (7)$$

where H is the atomic Hamiltonian and E_v is the exact eigenenergy of the atomic state. Applying e^{-T} on the preceding equation, we get

$$\bar{H}(1 + S)|\Phi_v\rangle = E_v(1 + S)|\Phi_v\rangle, \quad (8)$$

where

$$\bar{H} = H + \{\overline{HT}\} + \frac{1}{2!}\{\overline{HTT}\} + \frac{1}{3!}\{\overline{HTTT}\} + \frac{1}{4!}\{\overline{HTTTT}\}, \quad (9)$$

is the dressed Hamiltonian, $\{\cdots\}$ denotes normal ordering of the operators, and $\{\overline{A \cdots B}\}$ represents contraction between two operators A and B. The cluster amplitude equations of the singles and doubles are obtained after projecting Eq. (8) on singly and doubly replaced states $\langle\Phi_v^p|$ and $\langle\Phi_{va}^{pq}|$. From Wick's theorem and the normal ordered form of Hamiltonian ($H_N = H - \langle\Phi_v|H|\Phi_v\rangle = H - E_v^{(0)}$), we get after the projection

$$\langle\Phi_v^p|\bar{H}_N + \{\overline{\bar{H}_N S_1}\} + \{\overline{\bar{H}_N S_2}\}|\Phi_v\rangle = \Delta E_v^{\text{att}}\langle\Phi_v^p|S_1|\Phi_v\rangle, \quad (10)$$

$$\langle\Phi_{va}^{pq}|\bar{H}_N + \{\overline{\bar{H}_N S_1}\} + \{\overline{\bar{H}_N S_2}\}|\Phi_v\rangle = \Delta E_v^{\text{att}}\langle\Phi_{va}^{pq}|S_2|\Phi_v\rangle. \quad (11)$$

In these equations, ΔE_v^{att} is the valence correlation energy. It is defined as

$$\Delta E_v^{\text{att}} = \Delta E_v^{N,\text{corr}} - \Delta E_v^{N-1,\text{corr}}, \quad (12)$$

where $\Delta E_v^{N,\text{corr}}$ and $\Delta E_v^{N-1,\text{corr}}$ are the total and core correlation energies, respectively.

The right-hand sides of Eqs. (10) and (11) are what distinguish the open-shell coupled-cluster theory from the closed-shell coupled-cluster theory. These are the equivalent of the folded diagrams in the many-body perturbation theory (MBPT) of open-shell systems.

A. Energy eigenvalue

To obtain the energy eigenvalue E_v of the state $|\Psi_v\rangle$, we project Eq. (8) on the state $\langle\Phi_v|$, which gives

$$\langle\Phi_v|\bar{H}(1 + S)|\Phi_v\rangle = E_v, \quad (13)$$

where we have used $\langle\Phi_v|S|\Phi_v\rangle = 0$. Using the normal ordered Hamiltonian, defined earlier, Eq. (13) can be written as

$$\langle\Phi_v|[\bar{H}_N + E_v^{(0)}](1 + S)|\Phi_v\rangle = E_v. \quad (14)$$

From Wick's theorem,

$$\langle\Phi_v|[\bar{H}_N + \{\overline{\bar{H}_N S}\}]|\Phi_v\rangle = \Delta E_v^{N,\text{corr}}. \quad (15)$$

The attachment energy is the difference in the exact energy of the N- and $(N - 1)$-electron state (closed shell). In terms of correlation energies, attachment energy

$$E_v^{\text{att}} = \Delta E_v^{N,\text{corr}} - \Delta E_v^{N-1,\text{corr}} + \epsilon_v, \quad (16)$$

where ϵ_v is the single-electron energy of the valence electron.

From the closed-shell coupled-cluster theory, the correlation energy $\Delta E_v^{N-1,\text{corr}}$ has contributions from the closed diagrams. The right-hand sides of the amplitude equations Eqs. (10) and (11) absorb this correlation energy as $\langle\Phi_{\cdots}^{\cdots}|\{\bar{H}_N S\}|\Phi_v\rangle$ is equivalent to $\Delta E_v^{N-1,\text{corr}}\langle\Phi_{\cdots}^{\cdots}|S|\Phi_v\rangle$. Then the diagrams that contribute to ΔE_v^{att} are the ones shown in Fig. 2.

B. Multiple-valence shells

It is relatively straightforward to calculate, from the single-valence CCSD theory described, the ground-state wave function and energy. Then the entire single-particle basis spaces consist of one valence orbital, and the remaining are core (occupied) and virtual (unoccupied). However, to calculate excitation energies, the excited atomic states and eigenvalues must be calculated. The trivial way is to solve the CCSD equations of each atomic state, ground and excited, separately. For example, to evaluate the $5d \, ^2D_{3/2}$ excitation energy of Ba$^+$ ion, the ground state $|6s \, ^2S_{1/2}\rangle$ and the excited state $|5d \, ^2D_{3/2}\rangle$ must be calculated, which translates to solving two sets of CCSD equations with $a_{6s}^\dagger|\text{Ba}^{2+}\rangle$ and $a_{5d_{3/2}}^\dagger|\text{Ba}^{2+}\rangle$ as reference states. Here $|\text{Ba}^{2+}\rangle$ is the closed-shell Ba^{2+} reference state.

A better approach is to solve the ground- and excited-state CCSD equations in a single calculation. Then the theory is
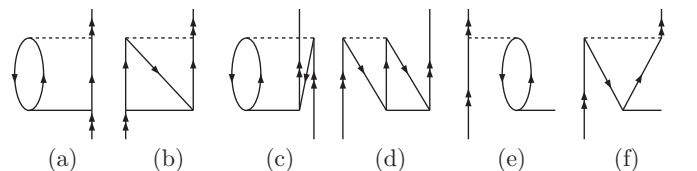

(a)   (b)   (c)   (d)   (e)   (f)

FIG. 2. Diagrams that contribute to ΔE_v^{att}. The dashed lines represent the residual Coulomb interaction.

multireference in nature and the cluster equations of different states are coupled. In the present case, we choose the model space to consist of one state of specific J and parity. Hence, we do not have to invoke a full-fledged multireference coupled-cluster theory.

III. PROPERTIES CALCULATION

A. Hyperfine structure constants

The hyperfine interaction H_{hfs} is the coupling of the nuclear electromagnetic moments to the electromagnetic field of the electrons. This causes splitting of the atomic levels and total angular momentum F is the conserved quantity. The atomic states are then $|(IJ)FM_F\rangle$, where I and J are the nuclear spin and total electronic angular momentum, respectively. The general form of the interaction is [20]

$$H_{\text{hfs}} = \sum_i \sum_{k,q} (-1)^q t_q^k(\hat{\mathbf{r}}_i) T_{-q}^k, \qquad (17)$$

where $t_q^k(\boldsymbol{r})$ and T_q^k are irreducible tensor operators of rank k effective in the electron and nuclear spaces, respectively. From the parity selection, only even and odd values of k are allowed for electric and magnetic interactions, respectively. For the magnetic dipole interaction ($k = 1$), the explicit form of the tensor operators are

$$t_q^1(\mathbf{r}) = \frac{-i\sqrt{2}[\boldsymbol{\alpha} \cdot \mathbf{C}_1(\hat{\mathbf{r}})]_q}{cr^2} \quad \text{and} \quad T_q^1 = \mu_q. \qquad (18)$$

Here $\mathbf{C}_1(\hat{\mathbf{r}})$ is a rank 1 tensor operator in electron space and μ_q is a component of $\boldsymbol{\mu}$, the nuclear magnetic moment operator. Then the nuclear moment is the expectation value of $\boldsymbol{\mu}$ in the stretched state $\mu = \langle II|\mu_0|II\rangle$. Parameters which represents the hyperfine splitting are the hyperfine structure constants. For one-valence atoms, the magnetic dipole hyperfine structure constant

$$a = \frac{g_I \mu_N}{\sqrt{j_v(j_v + 1)(2j_v + 1)}} \langle n_v \kappa_v || t^1 || n_v \kappa_v \rangle. \qquad (19)$$

Here, g_I ($\mu = g_I I \mu_N$) is the gyromagnetic ratio and μ_N is the nuclear magneton.

B. Hyperfine constants from coupled-cluster theory

The measured value of an atomic property A for the atomic state $|\Psi_v\rangle$ is the expectation

$$\langle A \rangle = \frac{\langle \Psi_v | A | \Psi_v \rangle}{\langle \Psi_v | \Psi_v \rangle}. \qquad (20)$$

In the present case, A is the hyperfine interaction H_{hfs} and in particular the magnetic dipole hyperfine interaction. From here on we use H_{hfs}; however, the derivations and discussions are general, applicable to any dynamical variable. When coupled-cluster wave functions, from Eq. (3), are chosen as the correlated atomic states,

$$\langle \Psi_v | H_{\text{hfs}} | \Psi_v \rangle = \langle \Phi_v | \tilde{H}_{\text{hfs}} + 2S^\dagger \tilde{H}_{\text{hfs}} + S^\dagger \tilde{H}_{\text{hfs}} S | \Phi_v \rangle, \qquad (21)$$

where, $\tilde{H}_{\text{hfs}} = e^{T^\dagger} H_{\text{hfs}} e^T$ is the dressed operator. The factor of two in the second term on the right-hand side accounts for $\tilde{H}_{\text{hfs}} S$ as $S^\dagger \tilde{H}_{\text{hfs}} = \tilde{H}_{\text{hfs}} S$. An expansion of $\tilde{H}_{\text{hfs}}$ ideal for an

orderwise calculation is

$$\tilde{H}_{\text{hfs}} = H_{\text{hfs}} e^T + \sum_{n=1}^{\infty} \frac{1}{n!} (T^\dagger)^n H_{\text{hfs}} e^T. \qquad (22)$$

The normalization factor [denominator in Eq. (20)], in terms of coupled-cluster wave function, is

$$\langle \Psi_v | \Psi_v \rangle = \langle \Phi_v | (1 + S^\dagger) e^{T^\dagger} e^T (1 + S) | \Phi_v \rangle. \qquad (23)$$

The dressed operator $\tilde{H}_{\text{hfs}}$ and operator $e^{T^\dagger} e^T$ in the normalization factor are nonterminating series. In the next section we describe a method for calculating $\tilde{H}_{\text{hfs}}$ to all orders in T iteratively.

IV. PROPERTIES TO ALL ORDERS

For accurate properties calculations it is appropriate to include higher-order terms in $\tilde{H}_{\text{hfs}}$. It is, however, nontrivial to go beyond the second order; the number of diagrams is large and a systematic evaluation is extremely tedious. On the other hand, diagrams can be grouped into different levels of excitation (LOE) and evaluated orderwise iteratively. Here LOE is the number of core or valence electrons replaced with virtual electrons. For example, the diagrams in Fig. 3 have LOE of 1. In each of these diagrams, one core electron is replaced by a virtual electron.

To calculate the diagrams of LOE 1 to all orders, consider the LOE 1 diagrams arising from $H_{\text{hfs}} e^T$, that is,

$$\left(H_{\text{hfs}} e^T \right)_1 = \left(H_{\text{hfs}} + \overline{H_{\text{hfs}} T} + \frac{1}{2} \overline{H_{\text{hfs}} T T} \right)_1, \qquad (24)$$

where the subscript denotes the LOE of the contributing terms. It is equivalent to a one-particle interaction and considered as an effective properties operator which incorporates electron correlations. In the next iteration,

$$\left(T^\dagger H_{\text{hfs}} e^T \right)_1 = \sum_i \left[T_i^\dagger \left(H_{\text{hfs}} + \frac{1}{2} \overline{H_{\text{hfs}} T} \right. \right.$$
$$\left. \left. + \frac{1}{6} \overline{H_{\text{hfs}} T T} \right) T_i \right]_1^{\text{conn}}, \qquad (25)$$

where $i = 1, 2$ in CCSD and the superscript conn implies that only the connected diagrams contribute. From the definition of the cluster operators, T_i and $T_i^\dagger$ have LOE i and $-i$,
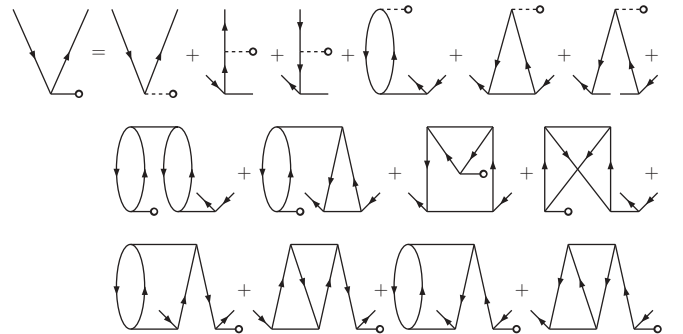

FIG. 3. Diagrammatic representation of the iterative equation for calculating the LOE 1 effective hyperfine operator $H_{\text{hfs}_1}^{\text{eff}}$. The iteration is implemented with $T_2^\dagger$ and T_2.
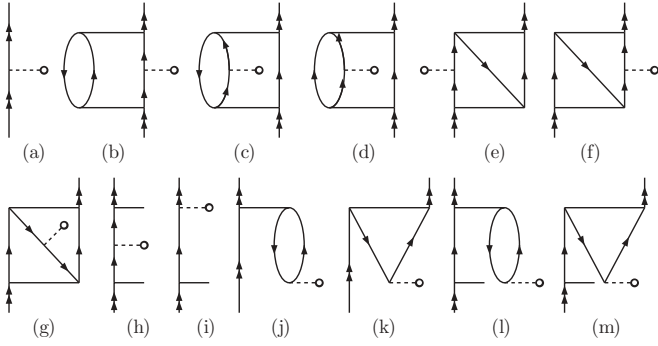
FIG. 4. Selected leading diagrams contributing to the hyperfine structure constants in Eq. (21). The dashed lines terminating with a circle represent hyperfine interaction.

respectively. The preceding equation is equivalent to the expression in Eq. (24) sandwiched between cluster operators of equal but opposite LOE. So the net LOE remains unchanged. In general, we can then write

$$(T^{\dagger n} H_{\mathrm{hfs}} e^T)_1 = \sum_i [T_i^\dagger (T^{\dagger n-1} H_{\mathrm{hfs}} e^T)_1 T_i]_1^{\mathrm{conn}}. \quad (26)$$

This is an iterative equation and it is possible to evaluate it order by order to convergence. The sum of all the contributions is equivalent to calculating the effective operator

$$\mathcal{H}_1 = (e^{T^\dagger} H_{\mathrm{hfs}} e^T)_1. \quad (27)$$

This contributes to the hyperfine structure as $S_2^\dagger \mathcal{H}_1$. At the lowest level, there are diagrams that correspond to Figs. 4(j) and 4(k). In a similar way, the effective properties of higher LOE are calculated.

For further study, we resort to diagrammatic analysis. Consider diagrams arising from $(H_{\mathrm{hfs}} e^T)_1$, there are six diagrams in total. These are shown on the first row on the right-hand side of Fig. 3. These define the initial choice of the effective diagram. For the next and higher iterations, consider the contractions with $T_2^\dagger$ and T_2. The contribution from $T_1^\dagger$ and T_1 is neglected as these cluster amplitudes, on an average, are several orders of magnitude smaller than T_2. Then the iteration is equivalent to the diagrammatic equation in Fig. 3 and it is mathematically

$$\mathcal{H}_1 = \mathcal{H}_1^0 + (T_2^\dagger \mathcal{H}_1 T_2)_1, \quad (28)$$

where $\mathcal{H}_1^0$ is $(H_{\mathrm{hfs}} e^T)_1$, the effective operator prior to the iteration. Since only the unique diagrams are considered, there are no multiplying factors. The algebraic relation in Eq. (28) is also without multiplying factors as the sequence of the contraction is uniquely defined, which is not the case in the expansion of $e^{T^\dagger} H_{\mathrm{hfs}} e^T$.

V. DESCRIPTION OF NUMERICAL METHODS

The calculations presented in this article involve various numerical techniques and methods. Some are fairly straightforward and often used in atomic theory calculations. Others are not and are specialized and application specific. For easy reference in future works, we provide an outline of the numerical methods used. This is appropriate as we

recommend, based on the current work, an approximation of the properties operator in coupled-cluster theory.

A. Atomic Hamiltonian and single-particle states

In the results presented in this article, the Dirac-Coulomb Hamiltonian is chosen H^{DC} for the calculations. It incorporates relativity at the single-particle level accurately, and, as the name indicates, the Coulomb interactions between the electrons. For an N electron atom

$$H^{\mathrm{DC}} = \sum_{i=1}^N [c\boldsymbol{\alpha}_i \cdot \boldsymbol{p}_i + (\beta - 1)c^2 - V_N(r_i)] + \sum_{i<j} \frac{1}{r_{ij}}, \quad (29)$$

where $\mathbf{p}$ is the linear momentum and α_i and β are the Dirac matrices. For the nuclear potential $V_N(r)$, we consider the finite-size Fermi density distribution

$$\rho_{\mathrm{nuc}}(r) = \frac{\rho_0}{1 + e^{(r-c)/a}}, \quad (30)$$

where, $a = t4\ln 3$. The parameter c is the half-charge radius, that is, $\rho_{\mathrm{nuc}}(c) = \rho_0/2$, and t is the skin thickness. At the single-particle level, the spin orbitals are of the form

$$\psi_{n\kappa m}(\boldsymbol{r}) = \frac{1}{r} \begin{pmatrix} P_{n\kappa}(r)\chi_{\kappa m}(\boldsymbol{r}/r) \\ i Q_{n\kappa}(r)\chi_{-\kappa m}(\boldsymbol{r}/r) \end{pmatrix}, \quad (31)$$

where $P_{n\kappa}(r)$ and $Q_{n\kappa}(r)$ are the large- and small-component radial wave functions, κ is the relativistic total angular momentum quantum number, and $\chi_{\kappa m}(\boldsymbol{r}/r)$ are the spin or spherical harmonics. One representation of the radial components is to define these as linear combination of Gaussian-like functions and are referred to as Gaussian-type orbitals (GTOs). Then the large and small components [21,22] are

$$P_{n\kappa}(r) = \sum_p C_{\kappa p}^L g_{\kappa p}^L(r),$$
$$Q_{n\kappa}(r) = \sum_p C_{\kappa p}^S g_{\kappa p}^S(r). \quad (32)$$

The index p varies over the number of the basis functions. For large component, we choose

$$g_{\kappa p}^L(r) = C_{\kappa i}^L r^{n_\kappa} e^{-\alpha_p r^2}, \quad (33)$$

where n_κ is an integer. Similarly, the small components are derived from the large components using the kinetic balance condition. The exponents in the preceding expression follow the general relation

$$\alpha_p = \alpha_0 \beta^{p-1}. \quad (34)$$

The parameters α_0 and β are optimized for each of the ions to provide good description of the properties. In our case the optimization is to reproduce the numerical result of the total and orbital energies. The optimized parameters used in the calculations are listed in Table I.

From Eq. (31) the reduced-matrix element of the magnetic hyperfine operator between two spin orbitals, v' and v, is

$$\langle v'||t^1||v\rangle = -(\kappa_v + \kappa_{v'})\langle -\kappa_{v'}||C^1||\kappa_v\rangle$$
$$\times \int_0^\infty \frac{dr}{r^2}\big(P_{n_{v'}\kappa_{v'}} Q_{n_v\kappa_v} + Q_{n_{v'}\kappa_{v'}} P_{n_v\kappa_v}\big). \quad (35)$$

A detailed derivation is given in Ref. [23].

TABLE I. Optimized parameters α and β of the GTO basis used in the calculations.

Symmetry	^{25}Mg$^+$			^{43}Ca$^+$			^{87}Sr$^+$			^{137}Ba$^+$		
	α	β	Basis function	α	β	Basis function	α	β	Basis function	α	β	Basis function
s	0.0083	2.8900	28	0.0063	2.8800	29	0.0083	2.9800	30	0.0063	2.9800	31
p	0.0072	2.9650	25	0.0072	2.9650	26	0.0072	2.9650	27	0.0072	2.9590	28
d	0.0070	2.7200	22	0.0070	2.7000	24	0.0070	2.8000	25	0.0070	2.4500	26

B. Basis set and cluster amplitudes

For all the alkaline-earth-metal ions considered, Mg$^+$, Ca$^+$, Sr$^+$, and Ba$^+$, we use V^{N-2} orbitals for the calculations. This is equivalent to calculating the spin orbitals from the single-particle eigenvalue equations of the doubly ionized alkaline-earth-metal atoms, namely, Mg^{2+}, Ca^{2+}, Sr^{2+}, and Ba^{2+}. Then the single-particle basis sets have few bound states and the rest are in the continuum. We optimize the basis such that single-particle energies of the core and valence orbitals are in good agreement with the numerical results. For this we use GRASP92 [24] to generate the numerical results.

As mentioned in earlier sections, we compute the closed-shell cluster amplitudes T first. These are used to generate the open-shell cluster amplitudes S. The coupled nonlinear and linear equations are solved iteratively. We employ direct inversion in the iterated subspace (DIIS) [25] for convergence acceleration.

VI. RESULTS AND DISCUSSIONS

A. Ionization potential and excitation energies

To determine the quality of the basis set and parameters, we compute the attachment energies of the ground state ($S_{1/2}$) and the first excited states, $P_{1/2}$, $P_{3/2}$, $D_{3/2}$, and $D_{5/2}$, are calculated. Then the ionization potential (IP), the energy required to remove the valence electron, is the negative of the attachment energy $-E^{\text{att}}$. To calculate the excitation energy (EE) of the state $|\Psi_v\rangle$, we consider E_g^{att} and E_v^{att} as the attachment energies of the ground state and the excited state, respectively. The difference $E_v^{\text{att}} - E_g^{\text{att}}$ is the EE, which can also be defined in terms of IPs.

For further analysis on the correlation effects incorporated with CCSD, we first compute IP with relativistic MBPT. The MBPT calculations are similar to our previous work [26] for second-order correlation energy of closed-shell atoms, in particular noble gas atoms. The MBPT diagrams of IP are similar to the first four attachment diagrams in Fig. 2 but have residual interaction instead of S and T operators, where, Figs. 2(a) and 2(b), direct and exchange, respectively, have the valence replaced by a virtual state and encapsulates core-valence correlation. Figures 2(c) and 2(d) represent core-core correlation as these involve double replacement of core electrons. Figures 2(e) and 2(f) with T_1 do not contribute as single replacements with residual Coulomb interaction are zero.

The results of the MBPT calculations are listed in Table II. The $3d$ $^2D_{3/2,5/2}$ and $3p$ $^2P_{1/2,3/2}$ of Mg$^+$, evaluated from the MBPT IPs, are marginally lower than the experimental data but are very close. From Ca$^+$, there is a change in the pattern of the EEs. The MBPT results of $^2D_{3/2,5/2}$ EEs are lower than

the experimental data, whereas the $^2P_{1/2,3/2}$ EEs are higher. The same pattern occurs in Sr$^+$ and Ba$^+$. A similar pattern is observed in the results of previous calculations [28]. The differences between the results in Ref. [28] and ours are minor and random in nature. These deviations can be attributed to the nature and completeness of the basis sets chosen in the two calculations.

The CCSD results of the EE are also listed in Table II, these are closer to the experimental data than the MPBT results. This is not surprising as CCSD encapsulates electron correlations more accurately. The trend of the CCSD results separates into two: Mg$^+$ and other ions. The additional electron correlation increases the IPs of Mg$^+$, whereas there is a decrease in the IPs of Ca$^+$, Sr$^+$, and Ba$^+$. However, the states change differently such that the EE improves. These results vouch for the reliability of the basis set for properties calculations.

B. Magnetic dipole hyperfine constants

To compute the hyperfine constants from the CCSD wave functions, we use Eq. (21). The results are listed in Table III; for comparison the results of other theoretical calculations and experimental data are also given. As defined in Eq. (21), the coupled-cluster expression of the hyperfine structure constants is separated into three groups. The dominant contribution from the first term $\tilde{H}_{\text{hfs}}$, up to first order in $T^\dagger$ and T, is

$$\tilde{H}_{\text{hfs}} \approx H_{\text{hfs}} + 2H_{\text{hfs}}T_1 + T_1^\dagger H_{\text{hfs}}(T_1 + 2T_2) + T_2^\dagger H_{\text{hfs}}T_2.$$

(36)

Here, the first term is the Dirac-Fock (DF), which has the largest contribution. The factor two in the second and fourth terms accounts for the complex conjugate terms. The third term, second order in T_1, has one diagram and a negligibly small contribution. The diagrams arising from the last term are topologically similar to the attachment diagrams in Figs. 2(c) and 2(d), except with the $T_2^\dagger$ instead of residual Coulomb interaction and H_{hfs} inserted on one of the orbital lines. There are ten diagrams and contribution from these are labeled as $\tilde{H}_{\text{hfs}} - $ DF. The last two terms in Eq. (21) are approximated as

$$S^\dagger \tilde{H}_{\text{hfs}} \approx 2S^\dagger (H_{\text{hfs}}e^T)_1,$$

(37)

$$S^\dagger \tilde{H}_{\text{hfs}}S \approx S_1^\dagger H_{\text{hfs}}(S_1 + 2S_2) + S_2^\dagger H_{\text{hfs}}S_2.$$

(38)

Like in $\tilde{H}_{\text{hfs}}$, the factor of two is to account for the complex conjugate terms. The expression of $(H_{\text{hfs}}e^T)_1$ is as given in Eq. (24). The $S_2^\dagger H_{\text{hfs}}S_2$ term has contributions from the diagrams in Figs. 4(b)–4(g). These are topologically similar to in Figs. 2(a) and 2(b), except, like in $T_2^\dagger H_{\text{hfs}}T_2$, with $S_2^\dagger$ instead of residual Coulomb interaction and H_{hfs} inserted to

TABLE II. Ionization potential and excitation energies. For comparison other results and experimental values are also listed. All values are in atomic units.

| Ion | State | MBPT | | Coupled cluster | | Other works | | Expt. results Ref. [27] |
		IP	EE	IP	EE	IP	EE	EE
^{25}Mg$^+$	$3s_{1/2}$	-0.55156	0.0	-0.55203	0.0	-0.55252	0.0	0.0
	$3d_{3/2}$	-0.22652	0.32504	-0.22666	0.32537	-0.22677	0.32575[a]	0.32573
	$3d_{5/2}$	-0.22652	0.32504	-0.22668	0.32535	-0.22677	0.32575[a]	0.32574
	$3p_{1/2}$	-0.38922	0.16234	-0.38950	0.16253	-0.39003	0.16249[a]	0.16252
	$3p_{3/2}$	-0.38878	0.16278	-0.38917	0.16286	-0.38961	0.16291[a]	0.16294
^{43}Ca$^+$	$4s_{1/2}$	-0.43784	0.0	-0.43671	0.0	-0.43836	0.0	0.0
	$3d_{3/2}$	-0.37797	0.05987	-0.37601	0.06070	-0.37768	0.06068[b]	0.06220
	$3d_{5/2}$	-0.37762	0.06022	-0.37578	0.06093	-0.37731	0.06205[b]	0.06247
	$4p_{1/2}$	-0.32180	0.11604	-0.32128	0.11543	-0.32217	0.11619[b]	0.11478
	$4p_{3/2}$	-0.32075	0.11709	-0.32119	0.11552	-0.32111	0.11725[b]	0.11580
^{87}Sr$^+$	$5s_{1/2}$	-0.40788	0.0	-0.40573	0.0	-0.40839	0.0	0.0
	$4d_{3/2}$	-0.34236	0.06552	-0.33926	0.06647	-0.34279	0.06560[b]	0.06632
	$4d_{5/2}$	-0.34091	0.06697	-0.33827	0.06746	-0.34132	0.06707[b]	0.06760
	$5p_{1/2}$	-0.29793	0.10995	-0.29696	0.10877	-0.29838	0.11001[b]	0.10805
	$5p_{3/2}$	-0.29421	0.11367	-0.29425	0.11148	-0.29463	0.11376[b]	0.11171
^{137}Ba$^+$	$6s_{1/2}$	-0.37297	0.0	-0.36862	0.0	-0.37308	0.0	0.0
	$5d_{3/2}$	-0.35296	0.02001	-0.34758	0.02104	-0.35172	0.02136[b]	0.02221
	$5d_{5/2}$	-0.34872	0.02425	-0.34386	0.02476	-0.34748	0.02560[b]	0.02586
	$6p_{1/2}$	-0.27685	0.09612	-0.27483	0.09379	-0.27532	0.09776[b]	0.09232
	$6p_{3/2}$	-0.26882	0.10415	-0.26821	0.10041	-0.26946	0.10362[b]	0.10002

[a]Reference [31].
[b]Reference [28].

one orbital line. Diagrams arising from the remaining terms are also given in Fig. 4. Based on this grouping, the contributions are listed in Table IV. In the following we present a detailed comparison of our magnetic hyperfine constant results with the earlier ones. As discussed later, some of our results are the best match with experimental data. This is a thorough test for the starting point of our iterative procedure and the expression for properties calculation we recommend.

1. Mg$^+$

The experimental data are available only for the ground-state $3s\ ^2S_{1/2}$ [16]. However, theoretical results are available for the low-lying states $3s\ ^2S_{1/2}, 3p\ ^2P_{1/2}, 3p\ ^2P_{3/2}, 3d\ ^2D_{3/2}$, and $3d\ ^2D_{5/2}$. In the previous works, the calculations used relativistic MBPT [29,30] and linearized CCSD [31] using numerical and B-spline basis sets, respectively. These report the DF contributions for $3s\ ^2S_{1/2}$ as -466.4 [30] and -463 [29]. The latter is in excellent agreement with our result, -463.29. The other dominant terms are $S^\dagger \tilde{H}_{\text{hfs}}$ and $\tilde{H}_{\text{hfs}} - $ DF; contributions from these are -107.32 and -16.13, respectively. Total value of these three terms is -586.76, or 98% of the experimental value. Our total value of -596.78, after including $S^\dagger H_{\text{hfs}} S$, is 0.08% lower than the experimental value and is the best theoretical result.

For the $3p\ ^2P_{1/2}$ and $3p\ ^2P_{3/2}$ states, our DF values -76.98 and -15.24 are in very good agreement with the values -77 and -15.2 given in Ref. [29]. The two states have 20.6% and 16.3% contribution to the total value from $S^\dagger \tilde{H}_{\text{hfs}}$. This difference shows variations in the nature of correlation effects, predominantly core polarization. Our total values for

the two states are -103.0 and -19.55, which are in very good agreement with the previous results.

For the $3d\ ^2D_{3/2}$ and $3d\ ^2D_{5/2}$ states, our DF values are -1.26 and -0.54, respectively. Whereas, the values in a previous work [29] are -1.61 and -0.54. The results of $3d\ ^2D_{5/2}$ match perfectly but there is a significant difference in the results of $3d\ ^2D_{3/2}$. Our result of -1.26 is 28% lower in magnitude. The correlation effects, core-polarization in particular, are markedly different from the other states. Contribution from $S^\dagger \tilde{H}_{\text{hfs}}$ to $3d\ ^2D_{3/2}$ is 0.19 is 15% in magnitude of DF and opposite in sign. It is even more dramatic for $3d\ ^2D_{5/2}$; it is 0.65, which is larger than DF in magnitude and opposite in sign.

Considering that the calculations in Ref. [29] incorporate core polarization to all orders, we can extract the pair correlation effects. For the $3s\ ^2S_{1/2}$ state, the core polarization contributes -91. Subtracting this from our $S^\dagger \tilde{H}_{\text{hfs}}$ result, the pair correlation contribution to this term is -16.32. Adding the other terms as well, the total contribution from pair correlation is -43.82, which is less than the core polarization but not negligible. For the other states the core-polarization contributions are $-18, -3.7$, and 0.71 for $3p\ ^2P_{1/2}, 3p\ ^2P_{3/2}$, and $3d\ ^2D_{5/2}$, respectively. The corresponding pair correlation contribution are $-7.86, -0.62$, and -0.04. The pair correlation is negligible in last two states and we have not estimated for $3d\ ^2D_{3/2}$ as there is a large difference between our DF value and Ref. [29].

2. Ca$^+$

This is the most well-studied, experimentally and theoretically, singly ionized alkaline-earth-metal ion. There is a large variation in the experimental results of $4s\ ^2S_{1/2}$ and

TABLE III. Magnetic dipole hyperfine structure constants (in MHz) of ^{25}Mg$^+$, ^{43}Ca$^+$, ^{87}Sr$^+$, and ^{137}Ba$^+$ ions.

Ion	State	This work	Other works	Expt.
^{25}Mg$^+$	$3s_{1/2}$	−596.785	−597.6[l], −554[s], −(602 ± 8)[t]	−596.254[m]
	$3p_{1/2}$	−102.997	−103.4[l], −100[s]	
	$3p_{3/2}$	−19.546	−19.29[l], −19[s]	
	$3d_{3/2}$	−1.083	−1.140[l], −1.25[s]	
	$3d_{5/2}$	0.118	0.1196[l], 0.107[a], 0.17[s]	
^{43}Ca$^+$	$4s_{1/2}$	−808.126	−805.35[b], −819[g], −794.7[h], −806.4(2.5)[u]	−797.5(2.4)[c], −805(2)[d]
	$4p_{1/2}$	−142.782	−143.07[b], −148[g], −144.8[h], −143[s], −145.4(4)[u],	−158(3.3)[c], −145.5(1.0)[d], −142(8)[e], −145.4(0.1)[f]
	$4p_{3/2}$	−32.185	−30.50[b], −30.9[g], −29.3[h], −30[s], −30.4(4)[u]	−29.7(1.6)[c], −31.9(0.2)[d], −31.0(0.2)[f]
	$3d_{3/2}$	−45.294	−47.82[b], −52[g], −49.4[h], −47.3(3)[u]	−48.3(1.6)[e], −47.3(0.2)[f]
	$3d_{5/2}$	−4.008	−3.351[a], −3.55[b], −5.2[g], −4.2[h], −3.6(3)[u]	−3.8(0.6)[f], 3.8931(2)[v]
^{87}Sr$^+$	$5s_{1/2}$	−990.638	−10003.18[b], −1000[k]	−1000.5(1.0)[i]
	$5p_{1/2}$	−169.988	−178.40[b], −177[k], −175[s]	
	$5p_{3/2}$	−36.225	−35.11[b], −35.3[k] −30[s]	−36.0[i]
	$4d_{3/2}$	−44.320	−47.36[b], −46.7[k]	
	$4d_{5/2}$	2.168	2.156[a], 2.51[b], 1.1[k]	2.17[j]
^{137}Ba$^+$	$6s_{1/2}$	4021.721	4072.83[p]	4018.2[q]
	$6p_{1/2}$	705.039	736.98[p]	
	$6p_{3/2}$	130.191	130.94[p], 126[s]	126.9[o], 112.77[r]
	$5d_{3/2}$	185.013	192.99[n], 188.76[p], 215[o]	189.730[o], 170.88[r]
	$5d_{5/2}$	−12.593	9.39[n], −11.717[a], −18[o]	−12.028[o]

[a]Reference [37].
[b]Reference [32].
[c]Reference [38].
[d]Reference [39].
[e]Reference [40].
[f]Reference [41].
[g]Reference [42].
[h]Reference [43].
[i]Reference [44].
[j]Reference [18].
[k]Reference [34].
[l]Reference [31].
[m]Reference [16].
[n]Reference [33].
[o]Reference [45].
[p]Reference [35].
[q]Reference [46].
[r]Reference [47].
[s]Reference [29].
[t]Reference [30].
[u]Reference [10].
[v]Reference [48].

$4p\,^2P_{1/2}$, and less in the results of $4p\,^2P_{3/2}$, $3d\,^2D_{3/2}$, and $3d\,^2D_{5/2}$ states. On the other hand, the theoretical results exhibit significant variations for all the states except $4p\,^2P_{3/2}$. The DF values of $4s\,^2S_{1/2}$ reported in previous works are −589 [29] and −588.933 [32], which are calculated with numerical and B-spline basis sets, respectively. Our value −589.09 is in very good agreement with these results. The core-valence correlation from $S^\dagger\tilde{H}_{\text{hfs}}$ accounts for 22% of the total value. This is much larger than in Mg$^+$ (17%). On the other hand, core-core correlation, contribution from $\tilde{H}_{\text{hfs}} - $ DF, is smaller. Our total value −808.12 is marginally higher than the experimental values but lies between the other theoretical results.

In previous studies, DF values of the $4p\,^2P_{1/2}$ are −102 [29] and −101.492 [32]. Similarly, for $4p\,^2P_{3/2}$ the values are −19.2 [29] and −19.646 [32]. These are in very good agreement with our results −101.47 and 19.65. As in $4s\,^2S_{1/2}$, there is an increase, compared to Mg$^+$, in $S^\dagger\tilde{H}_{\text{hfs}}$ contribution. It accounts for 26% and 30% of the total value for the two states. Our total values of $4p\,^2P_{1/2}$ is lower than the other theoretical results, whereas $4p\,^2P_{3/2}$ exhibits opposite trend.

For $3d\,^2D_{3/2}$, the DF values in the previous studies are −33 [29], −33.206 [32], and −39.12 [33]. The first two compare well with our value −33.55. Similarly, our $3d\,^2D_{5/2}$ DF value −14.29 is in good agreement with the previous results −14 [29] and −14.144 [32]. There is a change in the nature of

TABLE IV. Contributions from different terms in the coupled-cluster, magnetic dipole hyperfine constant properties expression. The values listed are in MHz.

Ion	State	DF	$\tilde{H}_{\mathrm{hfs}}$-DF	$S^{\dagger}\tilde{H}_{\mathrm{hfs}}$ +c.c.	$S_2^{\dagger}\tilde{H}_{\mathrm{hfs}}S_1$ +c.c.	$S_1^{\dagger}\tilde{H}_{\mathrm{hfs}}S_1$	$S_2^{\dagger}\tilde{H}_{\mathrm{hfs}}S_2$	Norm
					Coupled-cluster terms			
^{25}Mg$^+$	$3s_{1/2}$	−463.297	−16.136	−111.099	−1.637	−0.396	−5.560	1.002
	$3p_{1/2}$	−76.984	−2.754	−21.951	−0.348	−0.089	−0.989	1.001
	$3p_{3/2}$	−15.242	−0.695	−3.340	0.000	−0.018	−0.277	1.001
	$3d_{3/2}$	−1.259	−0.007	0.186	0.004	−0.001	−0.008	1.001
	$3d_{5/2}$	−0.540	−0.003	0.648	0.017	−0.000	−0.004	1.001
^{43}Ca$^+$	$4s_{1/2}$	−589.087	−12.696	−196.519	−4.782	−1.802	−10.717	1.009
	$4p_{1/2}$	−101.473	−0.497	−39.042	−1.089	−0.446	−1.031	1.006
	$4p_{3/2}$	−19.648	−0.321	−11.094	−0.244	−0.094	−1.004	1.007
	$3d_{3/2}$	−33.554	−2.553	−7.464	−0.128	−0.260	−2.153	1.018
	$3d_{5/2}$	−14.294	−1.247	13.531	0.490	−0.111	−2.449	1.018
^{87}Sr$^+$	$5s_{1/2}$	−738.204	−3.667	−235.962	−5.980	−3.046	−15.027	1.011
	$5p_{1/2}$	−122.363	−0.675	−44.789	−1.199	−0.678	−1.446	1.007
	$5p_{3/2}$	−21.501	−0.398	−13.096	−0.353	−0.126	−1.043	1.008
	$4d_{3/2}$	−31.368	−3.084	−8.184	−0.263	−0.139	−1.979	1.016
	$4d_{5/2}$	−13.080	−1.626	18.484	0.473	−0.058	−1.991	1.016
^{137}Ba$^+$	$6s_{1/2}$	3003.105	−39.093	1003.841	27.452	17.598	66.108	1.014
	$6p_{1/2}$	504.196	−5.948	197.723	5.728	4.072	6.064	1.010
	$6p_{3/2}$	73.674	0.665	50.583	1.605	0.619	4.480	1.011
	$5d_{3/2}$	129.875	12.565	35.669	1.067	0.462	9.495	1.022
	$5d_{5/2}$	52.085	7.240	−80.381	−1.553	0.191	9.554	1.022

$S^{\dagger}\tilde{H}_{\mathrm{hfs}}$ contribution to $3d\ ^2D_{3/2}$. Unlike in Mg$^+$, it is in phase with DF and a similar trend is observed in Sr$^+$ and Ba$^+$ as well. The contribution from ($S^{\dagger}\tilde{H}_{\mathrm{hfs}}$ + c.c.) to $3d\ ^2D_{5/2}$ is the only one which is lower in magnitude than the DF value. In all the other ions (Mg$^+$, Sr$^+$, and Ba$^+$) DF values are lower in magnitude. The impact of core-core correlation is not large but not negligible. Our total value for $3d\ ^2D_{3/2}$ is lower than all the theoretical and experimental values. However, our result for $3d\ ^2D_{5/2}$ matches very well with the experimental data.

Taking the core-polarization results from Ref. [32] and following the procedure in Mg$^+$, we estimate the pair correlation effects. We get the pair correlation contributions as −108.61, −19.37, −4.25, −11.96, and −7.99 for the $4s\ ^2S_{1/2}$ and $4p\ ^2P_{1/2}$, $4p\ ^2P_{3/2}$, $3d\ ^2D_{3/2}$, and $3d\ ^2D_{5/2}$, respectively. Except for $4p\ ^2P_{3/2}$ and $3d\ ^2D_{3/2}$, these are in very good agreement with the pair correlation listed in Ref. [32]. Not surprisingly, our results for these two states deviate from the other theoretical and experimental data.

3. Sr$^+$

Experimental data are limited to $5s\ ^2S_{1/2}$, $4p\ ^2P_{1/2}$, and $4d\ ^2D_{5/2}$. However, several theoretical investigations have examined the hyperfine structure of Sr$^+$. The $5s\ ^2S_{1/2}$ DF value in earlier works are −735 [34] and −736.547 [32]. Our value −738.204 is higher than both of the values. There is a large contribution from $S^{\dagger}\tilde{H}_{\mathrm{hfs}}$. It is 22% of the total value and the same as that seen with $4s\ ^2S_{1/2}$ of Ca$^+$. The core-core correlation is less significant. Our total result is lower than the experimental data and other theoretical results.

The DF values of $5p\ ^2P_{3/2}$ from previous works are −122 [34] and −121.576 [32], and values for $5p\ ^2P_{3/2}$ are

−21.4 [34] and −21.331 [32]. These are less than our values −122.363 and −21.501. The core-core correlation effects are negligibly small, 0.3% of the total value. Compared to Ca$^+$ ($4p\ ^2P_J$), there is an enhanced role of $S^{\dagger}\tilde{H}_{\mathrm{hfs}}$ in $5p\ ^2P_{3/2}$. It accounts for 33% of the total value. Our total value for $5p\ ^2P_{1/2}$ is less than the previous theoretical results. However, the value of $5p\ ^2P_{3/2}$ is in excellent agreement with the experimental data.

The DF values of $4d\ ^2D_{3/2}$ from previous works are −31.2 [34], −31.126 [32], and −34.23 [33]. And values for $4d\ ^2D_{5/2}$ are −13.0 [34], −12.977 [32], and −14.27 [33]. These compare well with our values −31.368 and −13.080. There is a marked change in the role of $S^{\dagger}\tilde{H}_{\mathrm{hfs}}$ for the $4d\ ^2D_{5/2}$ state. It has larger magnitude (135%) than the DF value. Our total value for $4d\ ^2D_{3/2}$ is lower than the other theoretical values. However, $4d\ ^2D_{5/2}$ is in excellent agreement with the experimental data.

There are noticeable differences in the estimates of the core-polarization effects in the earlier works [32,34]. For example, the core-polarization contribution to $4d\ ^2D_{3/2}$ is estimated as −6.3 in Ref. [34], whereas it is −2.413 in Ref. [32]. For consistency of analysis, with the choice in Ca$^+$, we adopt the core-polarization results of Ref. [32] and estimate pair correlation effects in our results. These are −127.795, −24.241, −3.938, −11.235, and −6.594. After accounting for the difference in the DF results, the results for $5s\ ^2S_{1/2}$ and $4d\ ^2D_{5/2}$ are in very good agreement with those of Ref. [32].

4. Ba$^+$

Ba$^+$ is a candidate system, as mentioned earlier, for a technique for measuring parity nonconservation (PNC)

experiment [19]. In this context, theoretical study of Ba$^+$ hyperfine constants is very important. It is a good proxy for the PNC in ions or atoms arising from neutral weak currents. Except for $6p\ ^2P_{1/2}$, there are experimental data for the low-lying states and theoretical results are available for $6s\ ^2S_{1/2}$, $6p\ ^2P_{1/2}$, $6p\ ^2P_{3/2}$, $5d\ ^2D_{3/2}$, and $5d\ ^2D_{5/2}$. The DF values of $6s\ ^2S_{1/2}$ in previous calculations are 2929.41 [35] and 3055 [36]. Our result is 3003.105, significantly different from both of the values. The contribution from the core-core correlation $\tilde{H}_{\mathrm{hfs}} - DF$ is of opposite phase to the DF contribution. This is in contrast to the states we have discussed so far. The total value is in very good agreement with experimental data but significantly different from the other theoretical results. It has 23% contribution from $S^\dagger \tilde{H}_{\mathrm{hfs}}$.

The DF values of $6p\ ^2P_{1/2}$ and $6p\ ^2P_{3/2}$ in the previous work are 492.74 [35] and 71.84 [35], respectively, which are different from our values of 504.196 and 73.674, respectively. The core-core correlation $\tilde{H}_{\mathrm{hfs}} - DF$, as in $6s\ ^2S_{1/2}$, is of opposite phase for $6p\ ^2P_{1/2}$. The total results of the two states are 705.039 and 130.191, respectively. The first is lower than the previous theoretical result, and the latter is in very good agreement with the theoretical result but lower than the experimental data.

The DF values of $5d\ ^2D_{3/2}$ in the previous studies are 128.27 [35] and 139.23 [33], and for $5d\ ^2D_{5/2}$ the values are 53.213 [37] and 55.82 [33]. Our results are 129.875 and 52.085, which are closer to Ref. [35] and Ref. [37], respectively. The $S^\dagger \tilde{H}_{\mathrm{hfs}}$ contribution to $5d\ ^2D_{5/2}$ is large, 141% of the DF value and opposite in phase. Our total total values 185.013 and -12.592 are close to experimental data.

For Ba$^+$, except for the ground state, there are no systematic studies of core-polarization effects. The previous work of Ref. [35] uses methods, GTO basis, and relativistic coupled cluster, similar to what we have used in the present article. Comparing the two, there is a good correlation between different coupled-cluster terms for all the states except $6s\ ^2S_{1/2}$.

C. All order calculations

In the previous section we analyzed and compared our results with earlier ones in some detail. The majority of our results are in very good agreement with the experimental data, some are perhaps the best match. The earlier works chosen for comparison are based on diverse types of orbitals: numerical, finite discrete spectrum, B-spline, and GTO. These are an accurate representation of the tried and tested types of single orbital in atomic calculations. Similarly, there is a variation in the many-body methods: MBPT, MCDF-EOL, and coupled-cluster. This is a large data set for comparison. More importantly, among the ions considered there are large changes in the role of electron correlations. This choice is essential to deliberate on the consequence of higher-order terms and avoid erroneous inference from an incomplete sample. This sets the stage for a systematic appraisal of the higher-order terms in the properties calculations.

As discussed in Sec. IV, we implement the iterative method to calculate the hyperfine constant to all orders for LOE 1. To frame the iterative equation in terms of components, we define τ as c numbers in the second quantized representation of $\mathcal{H}$.

That is,

$$\mathcal{H} = \sum_{ij} \tau_i^j a_i^\dagger a_j + \sum_{ijkl} \tau_{ij}^{kl} a_k^\dagger a_l^\dagger a_j a_i + \cdots . \qquad (39)$$

Equation (28) then assumes the form

$$\begin{aligned}
\tau_a^p = {}& h_{pa} + h_{pq} t_a^q + h_{ba} t_b^p + h_{bq} \tilde{t}_{ab}^{pq} \\
& + \tau_b^q \tilde{t}_{bc}^{*qr} \tilde{t}_{ca}^{pr} + \tau_c^p t_{bc}^{*qr} \tilde{t}_{ab}^{qr} + \tau_a^r t_{bc}^{*qr} \tilde{t}_{bc}^{qp},
\end{aligned} \qquad (40)$$

where h_{ij} is the matrix element $\langle i|h_{\mathrm{hfs}}|j\rangle$ and $\tilde{t}_{ij}^{kl} = t_{ij}^{kl} - t_{ji}^{kl}$ is the antisymmetrized cluster amplitude. This is the equation we solve iteratively until convergence. After each iteration, we evaluate the contribution from the effective operator to the hyperfine constant $S_2^\dagger \mathcal{H}_1$. The results of our calculations are given in Table V. For most of the cases, the results converge to KHz accuracy after two iterations.

In terms of absolute changes, the largest is observed in $6s\ ^2S_{1/2}$ of Ba$^+$. For this state the zeroth iteration, arising from $\mathcal{H}_1^0$, as given in Table V, is 469.636. It converges to 467.450 at the second iteration and the change is -2.186, which is 0.5% of the zeroth iteration and 0.05% of the total value, whereas in terms of fractional change, the largest is $5d\ ^2D_{5/2}$. Upon convergence, the change is -0.702, which is 1.9% of zeroth iteration. However, this is 5.5% of the total value. This arises from the large cancellation between the DF and $S^\dagger \tilde{H}_{\mathrm{hfs}}$. Here, to obtain correct result, the iterated calculation should be applied to the other terms as well. Not very surprisingly, the changes in Mg$^+$, Ca$^+$, and Sr$^+$ which have lower Z are negligibly small.

Considering that iteration is implemented for the LOE which contributes maximally. Contributions from the other LOEs are expected to be much smaller. Indeed, the contribution from LOE 0, as discussed in the next section is smaller by more than order of magnitude.

D. Error estimates

There are three important sources of error for the results listed in Table III. These are omission of higher-l basis states, truncation of the dressed properties operator in Eq. (22), and truncation of the cluster operator in Eq. (4). In the following we analyze and estimate the upper bound on the error arising from each of these sources.

The values in Table III are the converged results for basis functions up to the h symmetry. To estimate the contributions from higher symmetries, we include i symmetry and compute the hyperfine interaction constant. The largest contributions from i symmetry to $^2S_{1/2}$, $^2P_{1/2}$, and $^2P_{3/2}$ states are observed in Ba$^+$ and the changes are 0.01%, 0.06%, and 0.10% respectively. For the $^2D_{3/2}$ and $^2D_{5/2}$ states, the largest changes occur in the values of Mg$^+$, and these are 0.19% and 5.29%, respectively. In the present implementation of relativistic coupled-cluster theory, incorporating j and higher symmetry basis states renders the basis set too large for computations. However, a leading-order analysis is possible with MBPT and we find the contribution from j symmetry is negligible.

To estimate the error arising from the truncation of the dressed operator properties, we examine the higher-order terms computed with the iterative scheme. From Table V, the largest contributions from the LOE one are 0.11%, 0.28%, 0.40%, 0.36%, and 11.11% for the $^2S_{1/2}$, $^2P_{1/2}$, $^2P_{3/2}$, $^2D_{3/2}$, and $^2D_{5/2}$

TABLE V. Magnetic dipole hyperfine structure constant, contributions from higher-order terms in the all-order scheme [Eq. (22)].

Ion	State	$S^\dagger \tilde{H}_{\mathrm{hfs}}$				
		$(H_{\mathrm{hfs}}e^T)_1$	$T_2^\dagger (H_{\mathrm{hfs}}e^T)_1 T_2$	$T_2^{\dagger 2}(H_{\mathrm{hfs}}e^T)_1 T_2^2$	$T_2^{\dagger 3}(H_{\mathrm{hfs}}e^T)_1 T_2^3$	Converged value
^{25}Mg$^+$	$3s_{1/2}$	−53.663	−53.502	−53.503	−53.503	−53.503
	$3p_{1/2}$	−10.627	−10.563	−10.564	−10.564	−10.564
	$3p_{3/2}$	−1.592	−1.577	−1.577	−1.577	−1.577
	$3d_{3/2}$	0.093	0.091	0.091	0.091	0.091
	$3d_{5/2}$	0.324	0.321	0.321	0.321	0.321
^{43}Ca$^+$	$4s_{1/2}$	−90.109	−89.776	−89.778	−89.778	−89.778
	$4p_{1/2}$	−18.757	−18.570	−18.574	−18.574	−18.574
	$4p_{3/2}$	−4.845	−4.792	−4.793	−4.793	−4.793
	$3d_{3/2}$	−3.851	−3.887	−3.885	−3.885	−3.885
	$3d_{5/2}$	6.715	6.638	6.639	6.639	6.639
^{87}Sr$^+$	$5s_{1/2}$	−109.153	−108.716	−108.720	−108.720	−108.720
	$5p_{1/2}$	−22.116	−21.908	−21.912	−21.912	−21.912
	$5p_{3/2}$	−6.006	−5.943	−5.944	−5.944	−5.944
	$4d_{3/2}$	−4.216	−4.267	−4.265	−4.265	−4.265
	$4d_{5/2}$	8.822	8.687	8.689	8.689	8.689
^{137}Ba$^+$	$6s_{1/2}$	469.636	467.423	467.450	467.449	467.449
	$6p_{1/2}$	98.036	97.052	97.075	97.074	97.074
	$6p_{3/2}$	22.917	22.655	22.660	22.660	22.660
	$5d_{3/2}$	18.959	19.161	19.150	19.150	19.150
	$5d_{5/2}$	−36.806	−36.092	−36.104	−36.104	−36.104

states, respectively. Although not mentioned in the article, we also implement the iterative scheme for LOE 0 and find the largest contributions are 0.01%, 0.01%, 0.02%, 0.05%, and 1.64% for the $^2S_{1/2}$, $^2P_{1/2}$, $^2P_{3/2}$, $^2D_{3/2}$, and $^2D_{5/2}$ states, respectively. The contributions from LOE 2 and higher involve higher-order terms in T, hence have smaller contribution than LOE 0.

It is possible to estimate the errors arising from neglecting triples and higher cluster operators with a perturbative calculation [26]. For this we use the results from previous works. The contribution from the triples reported in computations similar to ours, using relativistic coupled-cluster theory, are 0.08%, 0.10%, 0.11%, and 0.29% for the $^2P_{1/2}$, $^2P_{3/2}$, $^2D_{3/2}$, and $^2D_{5/2}$ states in Ca$^+$ [49]. For the $^2S_{1/2}$ state contribution from triples is negligible. A similar trend is expected for the other ions as well.

To put a bound on the error in the results of $^2S_{1/2}$, $^2P_{1/2}$, $^2P_{3/2}$, and $^2D_{3/2}$, we select and add the largest change from each of the sources. This gives a value of 0.70%, which can be considered as the upper bound on the error in the results of Mg$^+$, Ca$^+$, and Sr$^+$. For the heavier ion Ba$^+$, another important source of error is the Breit interaction. Based on previous work [50], this can contribute up to 0.2%; hence, 0.9% is the appropriate upper bound for Ba$^+$ results. For the $^2D_{5/2}$ state, which has large cancellations, a comprehensive analysis is necessary to arrive at a meaningful error estimate. We shall address this rigorously in a our future works.

VII. CONCLUSIONS

We have calculated, as well as surveyed and compared, the magnetic hyperfine structure constants of low-lying states of Mg$^+$, Ca$^+$, Sr$^+$, and Ba$^+$ available in the literature. For the

states $3s \, ^2S_{1/2}$ (^{25}Mg$^+$), $3d \, ^2D_{5/2}$ (^{43}Ca$^+$), $4d \, ^2D_{5/2}$ (^{87}Sr$^+$), and $6s \, ^2S_{1/2}$ (^{137}Ba$^+$), our results provides the best match with the experimental data. Furthermore, results for most of the other states are in very good agreement with the available experimental data.

The chosen systems have hyperfine constants with varying dependence on electron correlations. It is a suitable data set for examining the impact of higher-order terms in properties calculations with relativistic coupled-cluster theory. This is of paramount importance for high-precision properties calculations with relativistic coupled-cluster theory. Our study establish without any ambiguity that the higher-order terms are not important when the leading terms DF and $S^\dagger \tilde{H}_{\mathrm{hfs}}$ contribute coherently. However, when large cancellation occurs, as in $^2D_{5/2}$ state of alkaline-earth-metal ions, a consistent calculation of the different terms to equal orders is a must. Except for such cases, based on the present study, we recommend

$$\langle \Psi_v | H_{\mathrm{hfs}} | \Psi_v \rangle = \langle \Phi_v | H_{\mathrm{hfs}} + 2H_{\mathrm{hfs}}T_1 + T_1^\dagger H_{\mathrm{hfs}}(T_1 + 2T_2)$$
$$+ T_2^\dagger H_{\mathrm{hfs}} T_2 + 2S^\dagger (H_{\mathrm{hfs}}e^T)_1$$
$$+ S_1^\dagger H_{\mathrm{hfs}}(S_1 + 2S_2) + S_2^\dagger H_{\mathrm{hfs}}S_2 | \Phi_v \rangle \quad (41)$$

for calculating hyperfine and similar properties for single-valence systems. It is sufficient to include terms up to quadratic in T for properties calculations. Higher-order terms, all together, have less than 0.1% of the total value and can be neglected.

[1] F. Coester, Nucl. Phys. **7**, 421 (1958).

[2] F. Coester and H. Kümmel, Nucl. Phys. **17**, 477 (1960).

[3] G. Hagen, T. Papenbrock, D. J. Dean, and M. Hjorth-Jensen, Phys. Rev. Lett. **101**, 092502 (2008).

[4] H. S. Nataraj, B. K. Sahoo, B. P. Das, and D. Mukherjee, Phys. Rev. Lett. **101**, 033002 (2008).

[5] R. Pal, M. S. Safronova, W. R. Johnson, A. Derevianko, and S. G. Porsev, Phys. Rev. A **75**, 042515 (2007).

[6] T. A. Isaev, A. N. Petrov, N. S. Mosyagin, A. V. Titov, E. Eliav, and U. Kaldor, Phys. Rev. A **69**, 030501(R) (2004).

[7] R. F. Bishop, P. H. Y. Li, D. J. J. Farnell, and C. E. Campbell, Phys. Rev. B **79**, 174405 (2009).

[8] K. V. P. Latha, D. Angom, B. P. Das, and D. Mukherjee, Phys. Rev. Lett. **103**, 083001 (2009).

[9] L. W. Wansbeek, B. K. Sahoo, R. G. E. Timmermans, K. Jungmann, B. P. Das, and D. Mukherjee, Phys. Rev. A **78**, 050501(R) (2008).

[10] B. K. Sahoo, Phys. Rev. A **80**, 012515 (2009).

[11] C. Thierfelder and P. Schwerdtfeger, Phys. Rev. A **79**, 032512 (2009).

[12] B. K. Sahoo, B. P. Das, and D. Mukherjee, Phys. Rev. A **79**, 052511 (2009).

[13] D. Mukherjee, Pramana **12**, 203 (1979).

[14] S. Salomonson, I. Lindgren, and A.-M. Mårtensson, Phys. Scr. **21**, 351 (1980).

[15] I. Lindgren and J. Morrison, *Atomic Many-Body Theory*, edited by G. Ecker, P. Lambropoulos, and H. Walther (Springer-Verlag, Heidelberg, 1985).

[16] W. M. Itano and D. J. Wineland, Phys. Rev. A **24**, 1364 (1981).

[17] G. Kirchmair, J. Benhelm, F. Zähringer, R. Gerritsma, C. F. Roos, and R. Blatt, Phys. Rev. A **79**, 020304(R) (2009).

[18] G. P. Barwood, K. Gao, P. Gill, G. Huang, and H. A. Klein, Phys. Rev. A **67**, 013402 (2003).

[19] N. Fortson, Phys. Rev. Lett. **70**, 2383 (1993).

[20] C. Schwartz, Phys. Rev. **97**, 380 (1955).

[21] A. K. Mohanty and E. Clementi, Chem. Phy. Lett. **157**, 348 (1989).

[22] R. K. Chaudhuri, P. K. Panda, and B. P. Das, Phys. Rev. A **59**, 1187 (1999).

[23] W. R. Johnson, *Atomic Structure Theory: Lectures on Atomic Physics* (Springer Verlag, Berlin, 2007).

[24] F. A. Parpia, C. Froese Fischer, and I. P. Grant, Comput. Phys. Commun. **94**, 249 (1996).

[25] P. Pulay, Chem. Phys. Lett. **73**, 393 (1980).

[26] B. K. Mani, K. V. P. Latha, and D. Angom, Phys. Rev. A **80**, 062505 (2009).

[27] NIST Atomic Spectroscopic Database, http://physics.nist.gov/PhysRefData.

[28] C. Guet and W. R. Johnson, Phys. Rev. A **44**, 1531 (1991).

[29] J.-L. Heully and A.-M. Martensson-Pendrill, Phys. Scr. **31**, 169 (1985).

[30] S. Ahmad, J. Andriessen, and T. P. Das, Phys. Rev. A **27**, 2790 (1983).

[31] M. S. Safronova, A. Derevianko, and W. R. Johnson, Phys. Rev. A **58**, 1016 (1998).

[32] K.-z. Yu, L.-j. Wu, B.-c. Gou, and T.-y. Shi, Phys. Rev. A **70**, 012506 (2004).

[33] W. M. Itano, Phys. Rev. A **73**, 022510 (2006).

[34] A.-M. Martensson-Pendrill, J. Phys. B **35**, 917 (2002).

[35] B. K. Sahoo, G. Gopakumar, R. K. Chaudhuri, B. P. Das, H. Merlitz, U. S. Mahapatra, and D. Mukherjee, Phys. Rev. A **68**, 040501(R) (2003).

[36] S. Ahmad, J. Andriessen, K. Raghunathan, and T. P. Das, Phys. Rev. A **25**, 2923 (1982).

[37] B. K. Sahoo, C. Sur, T. Beier, B. P. Das, R. K. Chaudhuri, and D. Mukherjee, Phys. Rev. A **75**, 042504 (2007).

[38] A. T. Goble and S. Maleki, Phys. Rev. A **42**, 649 (1990).

[39] R. E. Silverans, L. Vermeeren, R. Neugart, and P. Lievens, Z. Phys. D **18**, 351 (1991).

[40] F. Kurth, T. Gudjons, B. Hiblert, T. Reisinger, G. Werth, and A-M. Martensson, Z. Phys. D **34**, 227 (1995).

[41] W. Nortershauer *et al.*, Eur. Phys. J. D **2**, 33 (1998).

[42] A.-M. Martensson-Pendrill and S. Salomonson, Phys. Rev. A **30**, 712 (1984).

[43] A.-M. Martensson-Pendrill, A. Ynnerman, H. Warston, L. Vermeeren, R. E. Silverans, A. Klein, R. Neugart, C. Schulz, and P. Lievens (ISOLDE Collaboration), Phys. Rev. A **45**, 4675 (1992).

[44] F. Buchinger *et al.*, Phys. Rev. C **41**, 2883 (1990).

[45] R. E. Silverans, G. Borghs, P. De Bisschop, and M. Van Hove, Phys. Rev. A **33**, 2117 (1986).

[46] W. Becker, W. Fischer, and H. Huhnermann, Z. Phys. **216**, 142 (1968).

[47] C. Hohle, H. Huhnermann, Th. Meier, and H. Wagner, Z. Phys. A **284**, 261 (1978).

[48] J. Benhelm, G. Kirchmair, U. Rapol, T. Körber, C. F. Roos, and R. Blatt, Phys. Rev. A **75**, 032506 (2007).

[49] B. K. Sahoo *et al.*, J. Phys. B **36**, 1899 (2003).

[50] A. Derevianko, Phys. Rev. A **65**, 012106 (2001).